DEBRIS FLOWS: Disasters, Risk, Forecast, Protection

Proceedings
of the 7th International Conference

Chengdu, China, 23–27 September 2024

Edited by
S.S. Chernomorets, K. Hu, K.S. Viskhadzhieva

Geomarketing LLC
Moscow
2024

СЕЛЕВЫЕ ПОТОКИ: катастрофы, риск, прогноз, защита

Труды
7-й Международной конференции

Чэнду, Китай, 23–27 сентября 2024 г.

Ответственные редакторы
С.С. Черноморец, К. Ху, К.С. Висхаджиева

ООО «Геомаркетинг»
Москва
2024

泥石流：
灾害、风险、预测、防治

會議記錄
第七届国际会议

中国成都, 2024年9月23日至27日

編輯者
S.S. Chernomorets, K. Hu, K. Viskhadzhieva

Geomarketing LLC
莫斯科
2024

УДК 551.311.8
ББК 26.823
С29

Debris Flows: Disasters, Risk, Forecast, Protection. Proceedings of the 7th International Conference (Chengdu, China). – Ed. by S.S. Chernomorets, K. Hu, K.S. Viskhadzhieva. – Moscow: Geomarketing LLC. 622 p.

Селевые потоки: катастрофы, риск, прогноз, защита. Труды 7-й Международной конференции (Чэнду, Китай). – Отв. ред. С.С. Черноморец, К. Ху, К.С. Висхаджиева. – Москва: ООО «Геомаркетинг», 2024. 622 с.

泥石流：灾害、风险、预测、防治. 會議記錄 第七届国际会议. 中国成都. 編輯者 S.S. Chernomorets, K. Hu, K.S. Viskhadzhieva. – 莫斯科: Geomarketing LLC. 622 p.

ISBN 978-5-6050369-6-8

Ответственные редакторы: С.С. Черноморец (МГУ имени М.В. Ломоносова), К. Ху (Институт горных опасностей и окружающей среды Китайской академии наук), К.С. Висхаджиева (МГУ имени М.В. Ломоносова).

Edited by S.S. Chernomorets (Lomonosov Moscow State University), K. Hu (Institute of Mountain Hazards and Environment, CAS), K.S. Viskhadzhieva (Lomonosov Moscow State University).

При создании логотипа конференции использован рисунок из книги С.М. Флейшмана «Селевые потоки» (Москва: Географгиз, 1951, с. 51).

Conference logo is based on a figure from S.M. Fleishman's book on Debris Flows (Moscow: Geografgiz, 1951, p. 51).

Detecting the debris flow frontal velocity by the mud droplets impinging on rigid surfaces

K.L. Huang, H.T. Chou

National Central University, Jhongli, Taiwan, China, profhtchou@gmail.com

Abstract. The surging front of the debris flow is fatal and may cause tremendous damage for buildings. The splashed mud droplets on the damaged buildings provide useful information to reconstruct the fontal velocity of the debris flow. This study examines the spreading process that occurs and the splatter patterns that form when a mud droplet impacts a solid surface at various angles and velocities. The impact velocities of the droplet and the impact angles were between 2.16–7.10 m/s and 15°–90°, respectively. MATLAB software, imaging software, and a high-speed camera were used to analyze the geometric properties of the resulting splatter. When the droplet impacted the surface at a higher impact angle, the lamella expanded in an almost circular fashion (W/L ≈ 1), and the spreading velocity decayed exponentially. By contrast, the aspect ratio decayed with time at lower impact angles. The aspect ratio (W/L) of the elliptic fingerprint of the impact droplet was close to the sine value of the impact angle, and the larger the impact angle, the more splatter were observed. The Area spreading ratio of the impact droplet on the surface is a function of Weber number and Reynolds number for different solid surfaces, and roughly independent of the impact angle. The result of the present study could contribute to understanding the impact condition of the debris-flow surges on structure surfaces.

Key words: *mud droplets, debris flow, frontal velocity, splatters, impact angle*

Cite this article: Huang K.L., Chou H.T. Detecting the debris flow frontal velocity by the mud droplets impinging on rigid surfaces. In: Chernomorets S.S., Hu K., Viskhadzhieva K.S. (eds.) Debris Flows: Disasters, Risk, Forecast, Protection. Proceedings of the 7th International Conference (Chengdu, China). Moscow: Geomarketing LLC, 2024, p. 189–199.

Определение скорости фронтальной части селевого потока по каплям грязи, ударяющимся о твердые поверхности

К.Л. Хуан, Х.Т. Чоу

Национальный центральный университет, Чжунли, Тайвань, Китай,
profhtchou@gmail.com

Аннотация. Надвигающийся фронт селевого потока смертельно опасен и может нанести огромный ущерб зданиям. Капли грязи, разбрызгиваемые на поврежденные здания, дают полезную информацию для определения скорости Чуни фронтальной части селя. В данном исследовании рассматривается процесс распространения селевой волны и брызги, образующиеся при ударе капель грязи о твердую поверхность под разными углами и с разной скоростью. Скорость удара капли и углы удара составляли 2,16–7,10 м/с и 15°–90°, соответственно. Для анализа геометрических свойств образовавшихся брызг использовались пакет MATLAB, программное обеспечение для создания изображений и высокоскоростная камера. Когда капля ударялась о поверхность под большим углом, она расширялась почти по кругу ($W/L \approx 1$), а скорость распространения затухала по экспоненте. Напротив, при меньших углах подхода к зданию соотношение сторон уменьшалось со временем. Аспектное соотношение (W/L) эллиптического отпечатка капли было близко к синусу угла удара, и чем угол больше, тем больше наблюдалось брызг. Коэффициент распространения ударной капли по поверхности зависит от числа Вебера и числа Рейнольдса для различных твердых поверхностей и практически не

зависит от угла удара. Результаты настоящего исследования могут способствовать пониманию условий удара селевой волны о поверхности конструкций.

Ключевые слова: *капли грязи, селевый поток, фронтальная скорость, брызги, угол падения*

Ссылка для цитирования: Хуан К.Л., Чоу Х.Т. Определение скорости фронтальной части селевого потока по каплям грязи, ударяющимся о твердые поверхности. В сб.: Селевые потоки: катастрофы, риск, прогноз, защита. Труды 7-й Международной конференции (Чэнду, Китай). – Отв. ред. С.С. Черноморец, К. Ху, К.С. Висхаджиева. – М.: ООО «Геомаркетинг», 2024, с. 189–199.

Introduction

Due to its destructive velocity and thickness, the debris-flow front accompanying giant boulders may be fatal for people and cause tremendous damage for buildings as shown in Fig. 1*a* [*Chou et al, 2023*]. The mud splatters left on the damaged building ceiling (Fig. 1*b*) depict the powerful surging front of the catastrophic debris flow in Nansalu Village, Kaoshiung City of Taiwan during Typhoon Morakot (2009/08/09). Those mud splatters left on the ceiling after the impact of droplets indicate that the inertial force dominates the spreading of the mud droplets rather than the gravity force. The trajectories and patterns of the splashed droplets provide useful information to reconstruct the fontal velocity of the debris flow.

a b

Fig. 1. The debris-flow front caused badly damage to a building in Nansula Village during Typhoon Morakot on 08/09/2009 (picture taken on 06/06/2013): a – the debris-flow front with boulders caused severe damage to the building during Typhoon Morakot (08/09/2009); b – the mud splatters remained on the inside ceiling of the damaged building

The concept of droplets spreading on the dry surface is widely applied in industrial and nonindustrial processes. The process of a droplet impacting on a dry surface exhibits several flow patterns such as spreading, splashing, receding and rebound due to the surface and fluid properties [*Riboo et al, 2001*]. Brochard and De Gennes [*1984*] observed the profile of spreading polymer as a spherical cap with a projecting macroscopic “foot”. [*Pasandideh-Fard et al, 1996*] used surfactants to investigate the capillary effect on the spreading lamella. Šikalo et al. [*2005*] investigated the effect of the impact parameters on the time evolution of the spreading factor and apex height of the spreading lamella on horizontal and inclined surfaces. Wildeman et al. [*2016*] showed that with high velocity and free-slip condition, one-half of the initial kinetic energy can be transformed into surface energy in the spreading process, independent of the impact parameters. Furthermore, Gordillo et al. [*2019*] derived an analytical solution to predict the unsteady flow in the thin film which expands outwards. Garcia-Geijo et al. [*2021*] derived a theoretical model to predict the time-evolving asymmetric shape of the thin liquid film spreading on the substrate. For larger values of the inclination angle, the thin film

has an elliptical shape during the spreading process. MacDonell [*1971*] related the impact angle to the ratio of minor length to the major length with sine function. Harmanis and Thoroddsen [*1996*] introduced the Impact Reynolds number, $Re_I = V(\pi^2\rho D^3/16\sigma)^{1/4}/\nu^{1/2}$ to scale the maximum spreading diameter and the number of fingers, where ν is the kinematic viscosity, D the droplet diameter, σ the surface tension and ρ the fluid density.

Lee et al. [*2005*] developed a simple model to estimate impact velocity and droplet diameter via bloodstain diameters and the number of spines around the rim of a bloodstain. The model was compared to the experiment result under different surface roughness, impact inertia, and droplet size. Kang and Ng [*2006*], Kang et l. [*2011*] studied the effect of impact angle on splat morphology of spraying plasma and spreading behavior by analyzing the aspect ratio (Ψ) and the spread factor of elliptical-shaped splats. However, the spreading processes of the mud droplets upon different surfaces are still not fully understood because of the complexity of their multiphase characteristics. The geometric features in both the dynamic, earlier stage and the final stage of the spreading process are explored in this study. The mud droplets are mixtures of water, flour and poster paint. The effect of surface inclined angle, impact velocity, and surface roughness are examined by experiments. Surfaces with different roughness and material properties such as brick, mirror and Teflon are used.

Experimental setup

The experimental setup is shown in Fig. 2. The droplet is manually discharged from a syringe and falls onto the substrate by gravity. The impact velocity V is determined by the falling height and was calculated by the formula which Lighthill [*1978*] suggested:

$$H = \frac{1}{2}\left(\ln\frac{B}{A_u} - \ln\left(\frac{B}{A_u} - V^2\right)\right)/A_u, \quad (1)$$

where H is the falling distance, $B = g\left(1 - \frac{\rho_a}{\rho}\right)$, $A_u = 0.33\frac{\rho_a}{\rho}/D$, ρ is the density of droplet, ρ_a is the density of air. Here the Reynolds number, $Re = \rho_a V D/\mu_a$, and μ_a is the dynamic viscosity of the air. Eq. (1) has been validified by Chen [*2003*] as shown in Fig. 3, and it is valid when $Re \leqq 2\times10^5$.

In the experiment, the impinging and spreading process were observed from both top and side view with a high-speed camera (IDT, XS-3 model, with the frame rates from 3352–9954 fps, and resolution 10–20 pixels/mm). The initial time t =0 is defined as the drop first contacted with the surface (time error is under 0.3 ms). The spreading process and final pattern of the spatters were photographed vertically to the solid plane. At each drop height, the tests repeat six times, to reduce the error (about 7%). The splatter images taken from the high-speed camera were further analyzed by the Matlab built-in algorithm, "Sobel", which can detect the edge of each splatter and record their coordinates in every image. After the edge detection process, the characteristic feature of the spreading drop/splatters (drop height, splatter width, and length) can be calculated by simple discriminant loops written in Matlab language.

Table 1 shows the surface properties of two surfaces. The standard deviation (Stdev) of surface roughness R_a implies the high irregularity of the mirror and brisk surface, and the equilibrium contact angle shows the wettability characteristic of the mirror and brisk surface. The test fluids include decane and a mixture of water, poster paint, and flour as shown in Table 2. Flour was chosen to be the suspended particles in the water since it can be distributed more uniformly than clay or other soil materials. Moreover, the droplet impact sequences of the clay-contained droplet are too blurred to be analyzed by the Matlab program. The surface tension and viscosity of the test fluid were measured by the du Nouy Ring method and rheometer (Anton Paar, MCR 51).

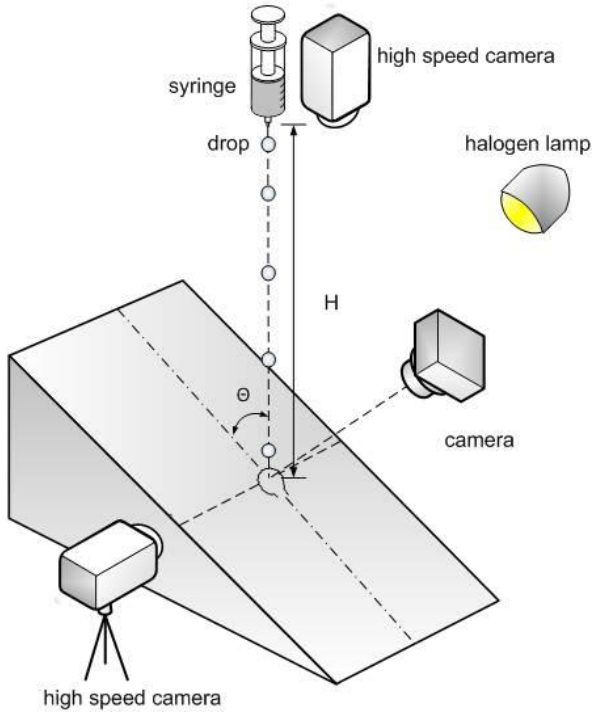

Fig. 2. Experimental setup

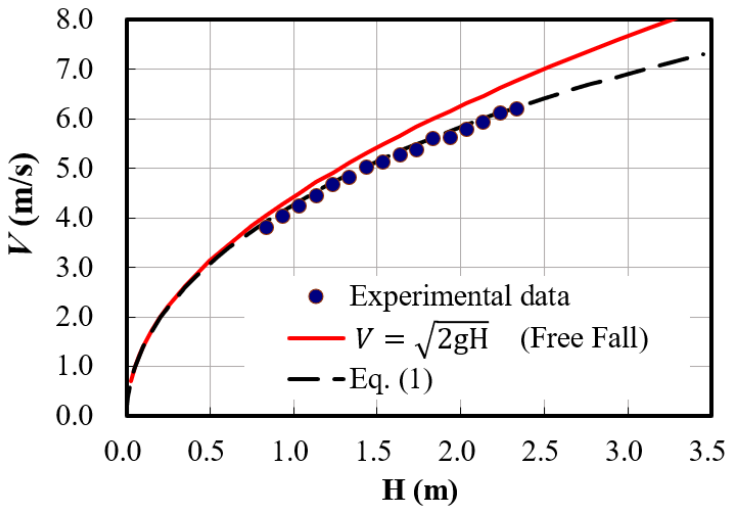

Fig. 3. The comparison between Eq. (1) and the experimental data from [*Chen, 2003*]

Table 1. Surface properties of impact surfaces

	R_a(μm)/Stdev	Receding contact angle, θ_r	Advancing contact angle, θ_a
Mirror	0.022/0.015	40∘	48∘
Brisk	25.8/8.03	34∘	44∘

Table 2. Liquid properties of tested fluid

Fluid	ρ (kg/m^3)	σ (dyne/cm)	μ (mPa·s)	D (mm)
Mixture	1170	51.3	11.0	4.71 ± 0.3
Decane	730	23.4	0.92	2.45 ± 0.15

Results and discussion

Morphology in the spreading process. Profile property of perpendicular impact droplet

Šikalo et al. [*2002*] showed how surface material, impact velocity, viscosity, surface tension, and droplet size affect the time evolution of apex height and spread factor. The result demonstrated surface property only affects the apex height in the recoil phase. The difference between the advancing and receding static contact angle of the test surface change from 0° to 105°, while the range of surface roughness, R_a is between 0.003 to 3.6 μm. Fig. 4*a* shows the side-view sequence when a droplet impacts the surface, and only deposition and splash were found under the present experiment condition. In the present study, drop height h was also normalized by droplet diameter D to h*=h/D, and time was normalized by (D/*V*) to t* = t*V*/D. Fig. 4*b* shows that impact velocity and surface did not affect the apex height evolution significantly, which gives the same result to Šikalos' study. The equation of fitting curve on mirror and brick is h*=-0.059+1.059exp(-1.23t*). The data is also compared with Roisman's [*2009*] approximation:

$$h^* \approx 1 - t^* \text{ at } t^* < 0.4, \tag{2}$$

which expresses the drop deposit almost as a rigid body at the beginning of spreading, and,

$$h^* \approx \frac{0.39}{(0.25+t^*)^2} \text{ at } 0.7 < t^* < t^*_{\text{viscous}}, \tag{3}$$

which ignores the near-wall boundary effect. The comparison shows the approximation fits well with experiment data after t* =0.8.

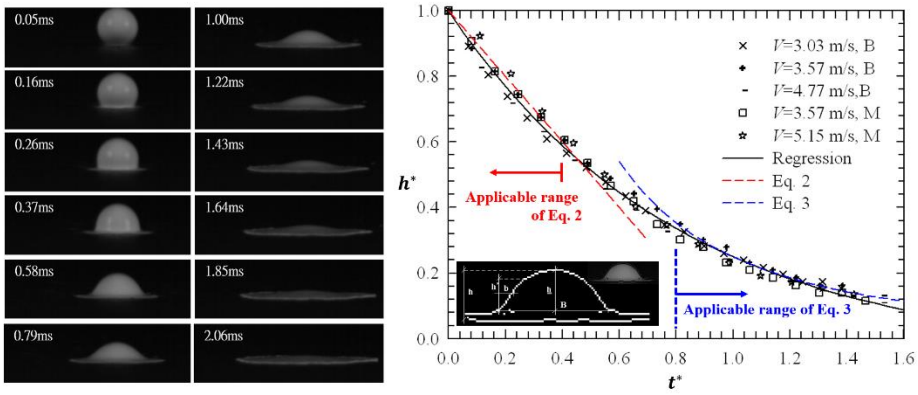

a b

Fig. 4. Sequence of photographs when the droplet impinging on the brisk surface (a). The evolution of dimensionless apex height during droplet spreading on different surfaces (×, +, -: brick surface; □, ☆: mirror surface), and with different impact velocities. The experiment data is compared with predicted equation suggested by Roisman et al. [*2009*]. Inset: Coordinate system of drop "hat" (b)

Because of the complicated interaction on the solid-liquid interface, a new analytical method was suggested in the study. The film region was ignored and the "hat" part was focused on. After the built-in edge detection function of Matlab, the contour coordinate was normalized by the central height of the droplet and the width of the "hat" part, which can be expressed as $h'^* = h'/h = f(x)$ and $b^* = \frac{b}{B} = x$ as defined in the inset of Fig. 4*b*. The results were compared with symmetric Beta distribution, which could be expressed as:

$$f(x) = \begin{cases} \frac{x^a(1-x)^a}{0.5^{2a}} & 0 \le x \le 1 \\ 0 & \text{elsewhere} \end{cases} \quad (4)$$

The experiment data fit well with Beta distribution, but the low resolution of the flatten hat makes contour data deviate from the function curve when t*>1. The parameter in Eq. (4) increases almost linearly with the dimensionless time t* (Fig. 5), showing the validity of Beta function in the velocity range of 2.41–5.15 m/s.

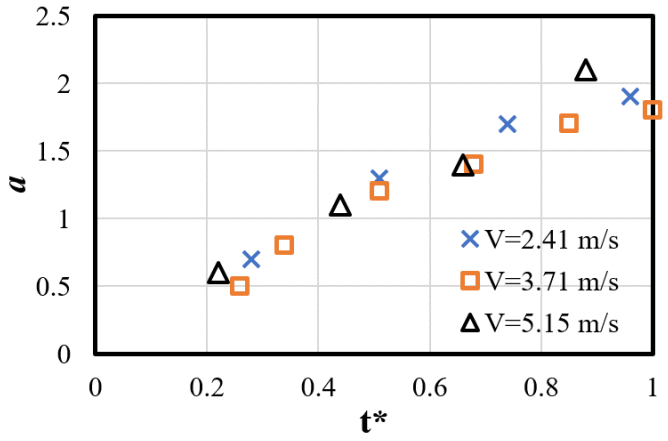

Fig. 5. The variation of parameter a in Beta function (Eq. 4) with t* at different impact velocity

Effect of impact angle on top-view contours

The time evolution of the spreading droplet contours on the inclined mirror with the impact velocity V =2.61m/s and different impact angles are shown in Fig. 6. During the spreading process, the expanding lamellas were elongated and gradually approached an elliptical shape. Ultimately, the liquid was accumulated by its own weight on the downside of the lamella. If the surface tension couldn't hold the accumulated liquid, it will flow down along the surface. Fig. 6 also shows upward spreading only occurs in θ =45°, 60°cases, and no receding occurs in four different impact angle conditions.

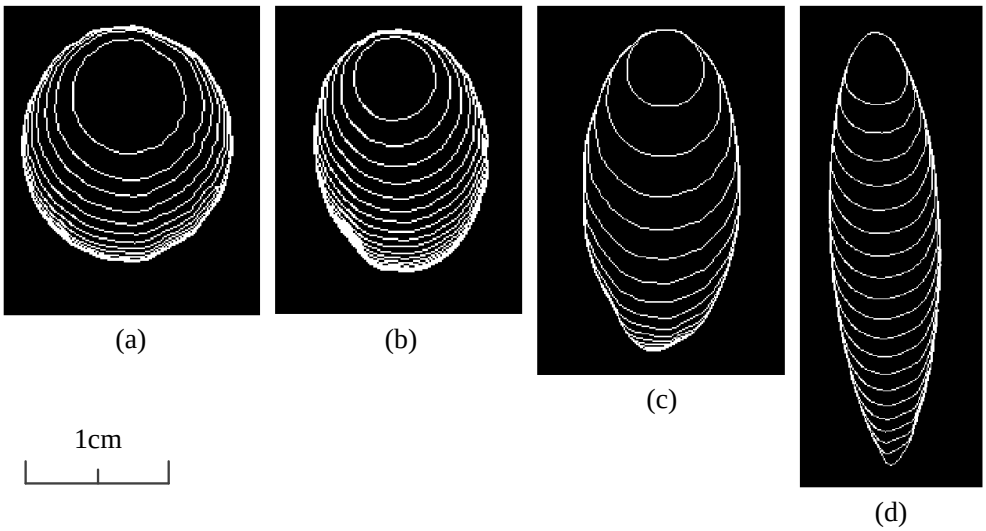

Fig. 6. Time evolution of expanding lamella contours with different impact angles at the impact velocity of V =2.61 m/s. The impact angles in (a) – (d) are 60°, 45°, 30°, 15°, respectively. The time intervals of neighboring contours in figures (a) – (d) are 0.54, 0.50, 0.53, 0.77 ms, respectively

In order to describe the contour evolution quantitatively, the major (L) and minor (W) axis of the contours were measured to define the aspect ratio, $I_f = 1/\Psi = W/L$ as Fig. 7*a* shown. Fig. 7*b* shows the effect of the impact angle on the aspect ratio of an expanding lamella. In cases $\theta = 45°, 60°$, the lamella first expanded circularly (W/L~1) in the initial state of the spreading process, then the aspect ratio decayed to a constant. In cases of lower impact angles such as $\theta = 15°, 30°$, the aspect ratio decayed from the very beginning of the spreading process. Ultimately, the aspect ratio of each splat approaches *sin*θ of the impact angle at different impact velocities.

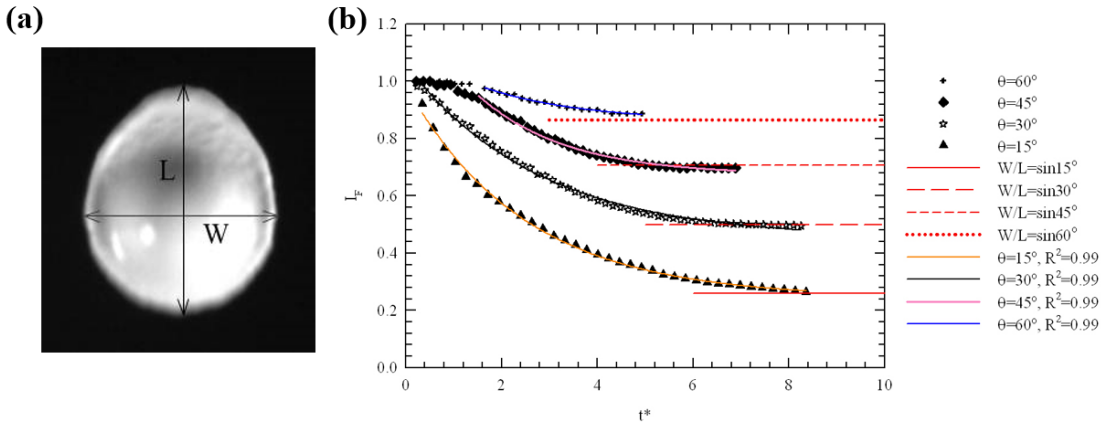

Fig. 7. Transience of a droplet spreading on an inclined mirror surface ($\theta = 30°$) (a). Time evolution of aspect ratio of expanding lamellas at different impact angles (V = 2.61m/s) (b)

Morphology of splatters

Fig. 8 shows the example of splatters left on both brick and mirror surfaces after impacting and spreading under different scenarios. Rough surface such as brick causes various splatter forms at different velocities, while splatters on mirror surfaces are more regular than that on brick. The sequence of the pictures as shown in Fig. 8*k* to Fig. 8*o* reveals the impact-angle effect on the development of splatters. Fingers are more active in the upper part of splatters than the lower part, and leakage occurs when the impact angle below 30° due to gravity effect.

The relationships between impact angles and number of fingers at different velocities are shown in Fig. 9. The number of fingers tends to increase linearly with *sin*θ, and the fitting equation for impact velocities of 2.41 m/s, 5.15 m/s and 6.70 m/s are $N_f = 24.5\ sin\theta - 7.5$, $N_f = 41.0\ sin\theta - 9.4$, and $N_f = 42.3\ sin\theta - 4.8$, respectively.

The geometric properties of splatters with fingers were based on their fingertips and the valleys, and the least-square method was applied to fit with an oval curve. The ultimate aspect ratio $I_{F(u)}$ was thus defined as W_u / L_u, where W_u and L_u are the minor and the major axis of the oval curve. Figs. 10*a–d* show the oval curve fits well with the splatters of lower impact angles, i.e., less the number of fingers. The splatter depicts an ellipse shape if all fingers were truncated. Fig. 10*e* shows ultimate transverse spread factor will increase linearly with *sin*θ, and the fitting equations of *V* =2.61 m/s and 5.15 m/s are $W_u/D = 1.67 + 3.34 sin\theta$ and $W_u/D = 1.32 + 2.02 sin\theta$, respectively.

The dimensionless splatter area A*, i.e. the ultimate spatter area ratio with respect to the droplet cross area ($A^* = \frac{splatter\ area}{\pi D^2/4}$), is a function of droplet inertia, surface tension, surface contact angle and liquid viscosity. A phenomenological model based on energy conservation was proposed by Pasandideh-Fard et al. [*1996*] as follows:

$$\frac{D_{splatter}{}^2}{D^2} = A^* = \frac{12+We}{3(1-cos\theta_a)+C(We/\sqrt{Re})}. \quad (5)$$

Fig. 8. Splatters left on different surfaces under different impact conditions. (a)~(e) represent on brick surface, V = 2.41 m/s, θ = 75°, 60°, 45°, 30°, 15°. (f)~(j) represent on brick surface, V = 5.15 m/s, θ = 75°, 60°, 45°, 30°, 15°. (k)~(o) represent on brick surface, V = 6.70 m/s, θ = 75°, 60°, 45°, 30°, 15°. (p)~(s) represent on mirror surface, V = 5.15 m/s, θ = 60°, 45°, 30°, 15°

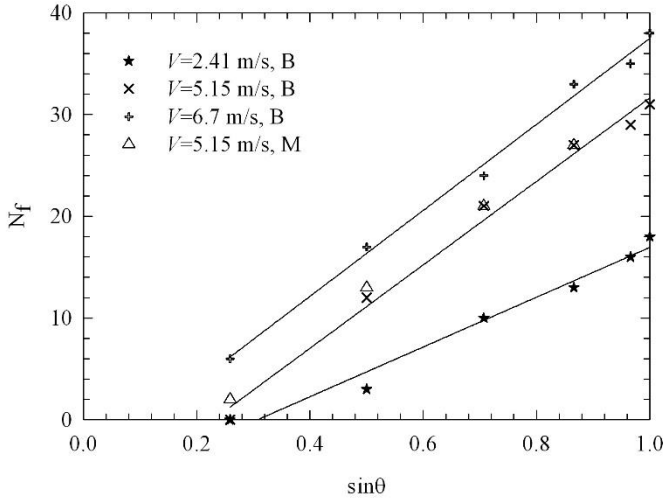

Fig. 9. The relationship between the impact angle and the number of fingers. Where ★, × – are brick surface; △ – mirror surface

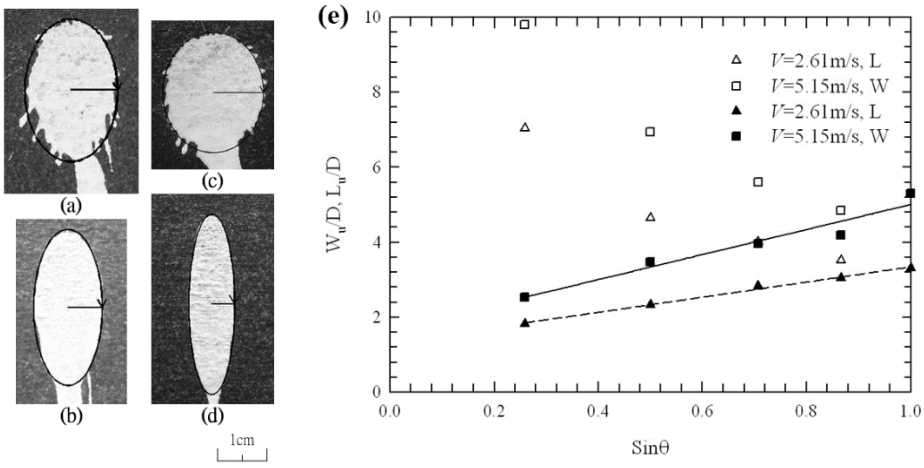

Fig. 10. The morphologic parameters of splatters under different impact conditions: a – H = 278 cm, θ = 45°; b – H = 150 cm, θ = 30°; c – H = 278 cm, θ = 60°; d – H = 29 cm, θ =15°; e – ultimate transverse spread factor of splatters on mirror surface as a function of the impact angle

In eq. (5), C is a constant representing the viscous dissipation and C= 4 was proposed in Pasandideh-Fard's et al. [*1996*] work.

By employing eq. (5) with the rheological properties and surface properties shown in Tables 1 and 2 (We $= \frac{\rho V^2 D}{\sigma}$, Re $= \frac{\rho V D}{\mu}$), one can predict the dimensionless splatter area A* with a constant C. The prediction with C = 2.7 in eq. (5) depicts better agreement with experimental data A^*_{exp} than the prediction with C = 4.0. The effect of surface roughness on A* seems negligible as shown in Fig. 11. Capillary effects tend to be negligible during droplet impact when We $\gg \sqrt{\text{Re}}$.

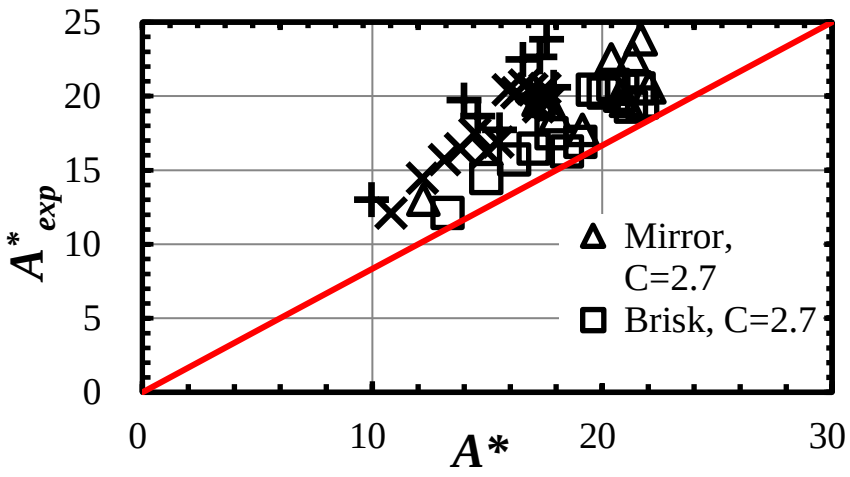

Fig. 11. The variation of dimensionless splatter areas (A^*) with Weber number (We) when droplets vertically impact brick and mirror surfaces

Fig. 12 shows the influence of impact angle on the splatter area of a pure liquid(decane). The influence of impact angle on dimensionless splatter area can be neglected for surfaces with larger equilibrium contact angles (θ_{eq}), thus the splatter area is mainly determined by the impact velocity corespondingly. However, the A^* values of smaller impact angles are larger than those of the normal impact cases ($\theta = 90^o$) for surafces with lower contact angles. The

corresponding mechanism for the conatct angles and liquid properties on the splatter spreading at different impact angles deserves further analysis.

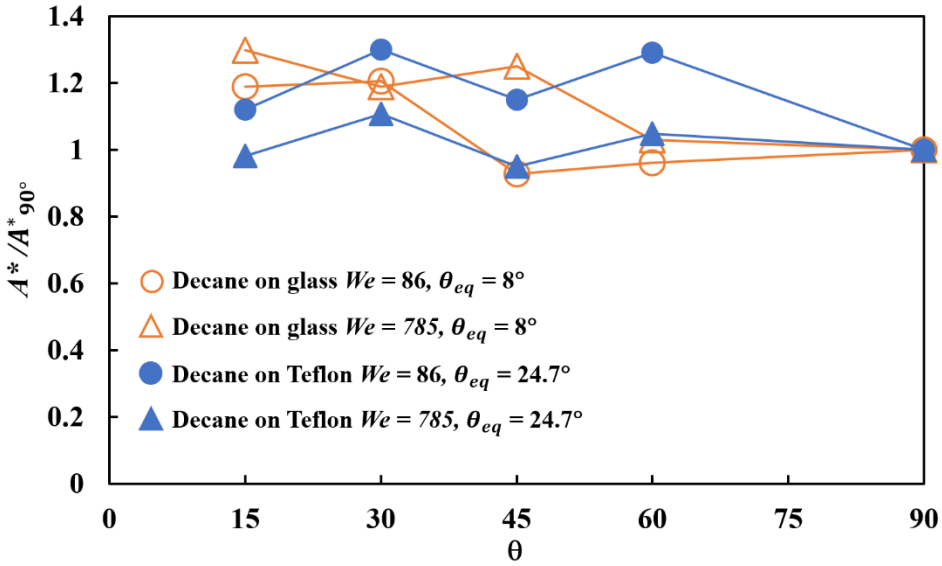

Fig. 12. The variation of the splatter area normalized by the that of normal impact ($A/A_{90°}$) with impact angle (θ) at different We and equilibrium contact angles

During the field investigation after the debris flow event, the dried splatter left on the building surface with its remained averaged thickness hf and the final spreading diameter D_{max}, which is correlated to the dimensionless splatter area A* as follows:

$$\frac{h_f/k}{D_{max}} = \frac{2}{3}\left(\frac{D}{D_{max}}\right)^3 = \frac{2}{3}A^{*\frac{3}{2}}. \quad (6)$$

In eq. (6), k denotes the solid volume concentration of the mud droplet prior to the inpingement. By employing eqs. (5) and (6) with the aspect ratio of the mud splatter remained on the surface and the droplet trajectory analysis, one can estimate the impact point and the corresponding debris-flow frontal velocity during its impingement on building surfaces.

Conclusion

The morphology of splatters and the spreading process were experimentally explored in this study, and the contribution of surface inclined angle, impact velocity and surface roughness to these features was investigated. In the initial state (t*<1) of the spreading process, the “hat” part of the droplet profile is closely fitted by the Beta function for perpendicular impact cases. When a droplet impacts an inclined surface, the lamella expands circularly in the initial state, then the aspect ratio(W/L) decays for cases of θ =45°, 60°; while the aspect ratio decays from the beginning of the spreading process for cases of θ =15°, 30°.The number of fingers and ultimate transverse spread factor of splatters increased linearly with *sin*θ. The aspect ratio for the elliptic fingerprint of the impact droplet is close to the sine value of the impact angle. The average length of fingers on the brick surface is larger than those on the mirror, and increasing impact velocity may wider the range of finger length in the brick surface case. The length distribution of fingers depicts a Maxwell-like distribution. The cohesion effect of the droplet on the splatter morphology could be studied further by using the clay droplet or larger concentrations of the added particles. The result of the present study could contribute to understanding the impact condition of the debris-flow surges on structure surfaces. The impact point and velocity of the debris flow on buildings could be estimated by the impact angles and splatter areas.

Acknowledgement

This research was partially funded by National Science Council, Taiwan, China (project numbers: 110-2625-M-008-008; 111-2222-E-008-007-MY2). The writers are grateful to Mr. Y.H. Chen and Ms. S.C. Hsieh for their help of performing droplet measurements.

References

Brochard, F. and de Gennes, P.G. [1984]. Spreading laws for liquid polymer droplets: interpretation of the <foot>. Journal of Physique Letters, 45, 597–602.

Bakshi, S., Roisman, I.V. and Tropea, C. [2007]. Investigations on the impact of a drop onto a small spherical target. Physics of Fluids, 19, 032102.

Chen, Y.H. [2003], On the relationship between geometric characteristics of mud splatters and the debris-flow front, Report of summer research project, National Science Council, Taiwan, R.O.C.)

Chou, H.T., Tsao, T.T., Hsu, C.H., Lee, C.F and Hwang, J.H., H.L., Lee, C.F. and Hwang, J.H. [2023]. Vulnerability assessment of buildings and residents for the catastrophic debris flow in Nansalu Village during Typhoon Morakot. Journal of Chinese Soil and Water Conservation, 54(1):72–81. (in Chinese)).

García-Geijo, P., Riboux, G. & Gordillo, J. M. [2020]. Inclined impact of drops", J. Fluid Mech., 897, A12.

Gordillo, J.M., Riboux, G., & Quintero, E. S. [2019]. A theory on the spreading of impacting droplets. Journal of Fluid Mechanics, 866, 298–315.

Kang, C.W. and Ng, H.W. [2006]. Splat morphology and spreading behavior due to oblique impact of droplets onto substrates in plasma spray coating process. Surface Coating Technology, 200(18–19), 5462–5477.

Kang C.W., Tan, J.K., Pan L., Lowb, C.Y., & Jaffar, A. [2011]. Numerical and experimental investigations of splat geometric characteristics during oblique impact of plasma spraying. Applied Surface Science, 257, 10363–10372.

Kannan, R. and Sivakumar, A. D. [2008]. Impact of liquid drops on a rough surface comprising microgrooves. Experiment of Fluids, 44, 927–938.

Lee, H.S., Mehdizadeh, N.Z. and Chandra, S. [2005]. Deducing drop size and impact velocity from circular bloodstains. Journal of Forensic Science 50(1), 54–63.

Lighthill, J. [1978], Waves in Fluids, Cambridge University Press, Cambridge, pp.226.

MacDonell, H.L. [1971]. Interpretation of bloodstains: Physical considerations. Legal Medicine Annual, C. Wecht, Ed., Appleton-century Crofts, New York.

Marmanis, H., and Thoroddsen, S.T. [1996]. Scaling of the fingering pattern of an impacting drop. Physics of Fluids, 8(6), 1344–1346.

Pasandideh-Fard, M., Qiao, Y. M., Chandra, S. & Mostaghimi, J. [1996]. Capillary effects during droplet impact on a solid surface. Phys. Fluids, 8(3), 650–659.

Rioboo, R., Marengo, M. & Tropea, C. [2001]. Outcomes from a drop impact on solid surfaces. Atomizatoin. Sprays, 11. 155–166.

Roisman, I.V., Berberović, E., & Tropea C. [2009]. Inertia dominated drop collisions. I. On the universal flow in the lamella. Physics of Fluids, 21, 052103.

Šikalo, Š., Marengo, M., Tropea, C. & Gani´c, E. N. [2002]. Analysis of impact of droplets on horizontal surfaces. Experimental Thermal and Fluid Science, 25, 503–510.

Wildeman, S., Visser, C. W., Sun C. & Lohse D. [2016]. On the spreading of impacting drops. Journal of Fluid Mechanics, 805, 636–655.